Published in final edited form as:
JACC Cardiovasc Imaging. 2013 December ; 6(12): . doi:10.1016/j.jcmg.2013.09.014.

The Advancing Clinical Impact of Molecular Imaging in Cardiovascular Disease

Eric A Osborn, MD PhD[1,2] and **Farouc A Jaffer, MD PhD**[2,3]

[1]Cardiology Division, Beth Israel Deaconess Medical Center, Harvard Medical School, Boston, MA

[2]Cardiovascular Research Center, Cardiology Division, Massachusetts General Hospital, Harvard Medical School, Boston, MA

[3]Center for Molecular Imaging Research and Wellman Center for Photomedicine, Massachusetts General Hospital, Harvard Medical School, Boston, MA

Abstract

Molecular imaging seeks to unravel critical molecular and cellular events in living subjects by providing complementary biological information to current structural clinical imaging modalities. In recent years, molecular imaging efforts have marched forward into the clinical cardiovascular arena, and are now actively illuminating new biology in a broad range of conditions, including atherosclerosis, myocardial infarction, thrombosis, vasculitis, aneurysm, cardiomyopathy, and valvular disease. Development of novel molecular imaging reporters is occurring for many clinical cardiovascular imaging modalities (PET, SPECT, MRI), as well in translational platforms such as intravascular fluorescence imaging. The ability to image, track, and quantify molecular biomarkers in organs not routinely amenable to biopsy (e.g. the heart and vasculature) open new clinical opportunities to tailor therapeutics based on a cardiovascular disease molecular profile. In addition, molecular imaging is playing an increasing role in atherosclerosis drug development in Phase II clinical trials. Here we present state-of-the-art clinical cardiovascular molecular imaging strategies, and explore promising translational approaches positioned for clinical testing in the near term.

Keywords

atherosclerosis; aneurysm; heart failure; molecular imaging; myocardial infarction; thrombosis; vascular injury; valvular disease

Introduction

Molecular imaging aims to delineate important biological disease processes that are invisible to traditional structural diagnostic imaging modalities. Clinical cardiovascular molecular

Correspondence: Farouc Jaffer MGH Cardiovascular Research Center Simches Research Building 3206 185 Cambridge Street Boston, MA 02114 Tel: 617.724.9353 Fax: 617.860.3180 fjaffer@mgh.harvard.edu.

Disclosures: FAJ - Research grant: Abbott Vascular, Merck, Kowa. EAO – none.

imaging efforts are increasingly providing new molecular and cellular insights into the *in vivo* biology of various cardiovascular diseases, including atherosclerosis, myocardial infarction, thrombosis, vasculitis, aneurysm, cardiomyopathy, and valvular disorders. Advances in these areas are improving our understanding of disease pathogenesis, and may illuminate new treatment targets and options for personalized disease monitoring and therapy. Recently, an expert panel from the National Heart, Lung, and Blood Institute Working Group convened to identify barriers to clinical translation within molecular imaging, and provided several recommendations for fostering further development of the field (1). In this review, we highlight recent advances in cardiovascular molecular imaging, encompassing studies published in 2011 and 2012, focusing on clinical applications and important translational preclinical advances. Key questions for the field include: (1) Will molecular imaging readouts translate into improved clinical risk stratification? and (2) Can molecular imaging predict the success or failure of new pharmacotherapies in early stages – to help streamline drug development?

Atherosclerosis

Molecular imaging aims to identify and guide treatment of vulnerable atherosclerotic plaques at high risk of rupture and subsequent thrombosis. Putative at-risk lesions display pathological features such as inflammation, thrombosis, neovessel formation, apoptosis, and hemorrhage, several of which are well suited to detection with molecular imaging agents (Table I). While non-invasive PET-based metabolism/inflammation plaque imaging with ^{18}F-fluorodeoxyglucose (FDG) dominates the current clinical landscape, emerging agents such as ^{18}F-sodium fluoride (NaF) for PET and new applications of MRI-detectable ultrasmall superparamagnetic particles of iron oxide (USPIO), among other innovations, are being explored. An overarching question that is being addressed is: will molecular imaging readouts provide additional risk prediction beyond clinical risk factor scores, blood biomarkers, and anatomical imaging?

Carotid plaque ^{18}F-fluorodeoxyglucose (FDG) PET imaging

FDG is a radiolabeled glucose analog that concentrates in metabolically active cells, and can be detected by positron emission tomography (PET) imaging. In atherosclerosis, FDG correlates with macrophage infiltration, as well plaque hypoxia, and overall serves as a surrogate marker of plaque inflammation. Although FDG PET imaging of plaque inflammation is generally restricted to larger arterial beds such as the carotid arteries and aorta, efforts to image the coronary arteries are emerging. Due to its widespread clinical availability, FDG-based PET/CT molecular imaging studies have dominated the atherosclerosis landscape.

Clinical associations of carotid plaque FDG signal elevation with cardiovascular risk factors—Factors associated with carotid FDG activity were assessed in a cross-sectional study of 82 subjects with stable coronary artery disease (CAD) (2), of which 95% were taking chronic statin therapy and 38% had diabetes. Quantitative carotid FDG uptake was assessed by multiple metrics including maximum whole vessel target-to-background ratios (TBR) and standardized uptake value (SUV). SUV was determined by measuring the local arterial FDG activity corrected for the injected FDG dose, and body weight or body surface area. However, because the target artery often contains plaque and luminal FDG-positive blood, an attempt to correct for residual background blood signal can be made by dividing the plaque artery SUV by the venous blood SUV, to generate a TBR value. Prior work from Rudd and Fayad et al. (*J Nucl Med* 2008) have shown that the mean and max TBRs are reproducible and suitable for atherosclerosis drug trials, although other correction methods, e.g. Plaque artery SUV –

venous SUV, might also be useful. In the current study, artery FDG SUVs and TBRs were correlated with traditional cardiovascular risk factors through multivariate linear regression analysis. The strongest predictors of carotid FDG uptake were obesity (BMI≥30kg/m^2) and age >65 years (both p≤0.01), followed by male gender and a history hypertension or smoking (all p≤0.05). Furthermore, the number of metabolic syndrome features present incrementally increased with carotid FDG activity. Interestingly the presence of diabetes alone was not predictive in this study, although a subsequent analysis of 43 noninsulin-dependent diabetic patients by the same investigators demonstrated a significant association between fasting glucose and carotid FDG uptake, after correction for the pre-scan blood glucose (3). The overall findings strengthen the likelihood that FDG-PET will identify high-risk plaques and patients. However, outcome studies will be needed to determine FDG plaque assessment improves risk prediction beyond risk factors.

Another CAD equivalent, peripheral arterial disease, did not show significant correlation between FDG uptake and immunohistological macrophage content in femoral arterial plaque samples obtained from 21 patients that underwent PET imaging within 2 weeks of catheter-based directional atherectomy (4). However, it is possible that these findings were limited by the sample collection method that precluded accurate FDG PET/CT co-registration.

Associations between carotid plaque FDG uptake and high-risk plaque morphology—Inflammation, expansive remodeling, lipid-rich necrotic core, and ulceration are high-risk features underlying plaque rupture. Associations between FDG inflammation and CT high-risk plaque morphological characteristics were examined in 34 patients with carotid stenosis (5). Compared to plaques without high-risk features, those demonstrating CT positive remodeling, luminal irregularity (ulceration), or low attenuation (lipid) had greater FDG PET activity (TBR 2.2 any marker, vs. 1.7 no marker, p<0.001). In addition, the carotid FDG signal increased as a function of the number of high-risk features present (p<0.001). Immunohistochemistry of CEA specimens demonstrated greater macrophage content in high FDG plaques that tracked with more high-risk morphology features (p<0.001). Future clinical atherosclerosis imaging risk stratification strategies are likely to be strengthened by combining molecular imaging data with detailed structural information on plaque morphology. These data extend the potential of FDGPET/CT to identify high-risk carotid plaques. However, in the next years FDG inflammation imaging will need show utility beyond anatomical imaging to become routinely clinically adopted.

Carotid plaque FDG and periodontal inflammation—Can the teeth serve as window to the health of the arteries? Severe periodontal disease is associated with adverse cardiovascular outcomes. To further understand the association between periodontal disease and atherosclerosis, 112 patients underwent jaw and large artery FDG imaging (6). The periodontal FDG signal correlated well with the carotid artery signal (r=0.64, p<0.001), and also to a lesser extent with aorta signal (r=0.38, p=0.029; Figure 1). In a subset of 16 patients that subsequently underwent CEA, FDG signals correlated well with plaque macrophages (r=0.81, p<0.001) further supporting FDG as a reporter of local tissue macrophage infiltration. This insight may motivate strategies to further understand whether periodontal disease could actually drive atherosclerosis (via the generation of a systemic inflammatory response), or vice versa, or whether preceding systemic inflammation drives both periodontal disease and atherosclerosis. This study could also help reinvigorate efforts to screen patients with poor periodontal health for cardiovascular disease.

FDG plaque uptake in a JUPITER-type primary prevention population—Mechanisms underlying the benefits of statins in patients with “normal” LDL levels remain unknown. Yoo and colleagues evaluated carotid FDG activity in 120 apparently healthy individuals stratified according to baseline high-sensitivity C-reactive protein (hsCRP) and

LDL values (7). The study design was similar to the JUPITER trial, which demonstrated a rosuvastatin-mediated reduction in cardiovascular events and all-cause mortality in those with "normal" LDL levels <130mg/dl, but with elevated systemic inflammation defined by hsCRP ≥2.0mg/L. Using these same cutoff strata, subjects with hsCRP≥2.0mg/L and low LDL<130mg/dl had greater carotid FDG signals than those with low hsCRP/low LDL, or low hsCRP/high LDL (maximum TBR: 1.29±0.13, 1.12±0.10, and 1.16±0.15, respectively; p<0.01). Notably, there were no differences in carotid ultrasound intima-media thickness (CIMT) among these groups. This exciting study provides new insights in that plaques can be inflamed despite a "normal" LDL level. Future studies need to inform whether local FDG plaque inflammation detection offers superior risk prediction beyond risk factors and the blood hsCRP level, a simpler and much less costly test.

Assessment of anti-inflammatory effects of anti-diabetes pharmacotherapy— Reduction of atheroma inflammation is hypothesized as a strategy to stabilize vulnerable plaques, and is being formally tested in large clinical trials using agents such as methotrexate (CIRT trial) and canakinumab (CANTOS trial). Identifying specific FDA-approved agents that exhibit plaque-specific anti-inflammatory effects, particularly in higher risk diabetic patients, could be of considerable importance. To this end, Mizoguchi et al. compared the anti-inflammatory properties of two anti-diabetic agents, pioglitazone (insulin sensitizing) and glimepiride (insulin secreting), in a serial FDG imaging trial of 56 randomized diabetic patients (8). Compared to pre-randomization baseline FDG imaging, the pioglitazone-treated group demonstrated significantly greater suppression of FDG carotid and aortic plaque inflammation compared to the glimepiride group (pioglizatone: ΔTBR −0.14, p<0.01; glimepiride: ΔTBR +0.06, p=NS, Figure 2). Notably each group showed similar reductions in fasting plasma glucose and hemoglobin A1c levels. This study extends prior preclinical imaging evidence of decreased inflammation observed with pioglitazone (9,10) and may underlie the favorable clinical and ultrasound imaging results observed in the PROactive, CHICAGO, and PERISCOPE clinical trials.

Anti-inflammatory effect of new lipid-modifying and anti-inflammatory therapeutics—Developing new phamacotherapies for CVD is of paramount importance but a time-consuming, costly endeavor. Agents that increase HDL levels appeared initially attractive, but recent experience with the cholesterylesterase transfer protein (CETP) inhibitor torcetrapib was associated with increased mortality attributed to off-target effects. Dalcetrapib, a new CETP inhibitor, was tested in the phase IIb, randomized, double-blind, placebo-controlled dal-PLAQUE trial that included atheroma characterization endpoints by serial carotid MRI and FDG PET imaging (11). At 6 months, dalcetrapib increased HDL levels by 34%. PET imaging demonstrated a modest nonsignificant trend towards decreased carotid FDG activity compared to controls (−7.3% TBR reduction, 90% CI −13.5 to −0.8). Serial MRI however showed a relative 4.0 mm^2 reduction in total carotid wall area at 24 months compared to baseline (dalcetrapib vs. control, p=0.04). In comparison to torcetrapib, dalcetrapib demonstrated a good safety profile without enhancing plaque progression or inflammation. However, despite these potentially encouraging findings, the dalcetrapib phase 3 study dal-OUTCOMES was recently halted for futility. Therefore the field of surrogate atherosclerosis imaging is still in need of a predictive champion. FDG PET has proven successful in showing statin-based reductions in plaque inflammation – but statins already were established with hard endpoints prior to such imaging trials. Perhaps both carotid imaging endpoints together – reduction of inflammation by FDG *and* reduction of plaque volume by MRI – will be more predictive of drug success, at least in reducing cerebrovascular events. Whether a non coronary artery-based molecular imaging method can accurately predict coronary events also remains to be determined.

Inflammation itself, independent of lipid-based modulation, is also a promising emerging therapeutic target. The "inflammatory hypothesis" will be tested clinically in clinical trials of low-dose methotrexate (CIRT), the interleukin-1β inhibitor canukinamab (CANTOS), and of other novel anti-inflammatory therapeutics. One new agent, losmapimod, which inhibits p38 mitogen-activated protein kinase intracellular inflammation pathways, was tested in 99 patients already on statin therapy randomized 1:1:1 to once or twice daily 7.5 mg losmapimod or placebo. Carotid and aorta inflammation was imaged with FDG PET/CT at baseline and 84 days later (12). Although averaging all analyzable segments demonstrated no significant relationships, secondary analysis restricted to segments with high FDG signal at baseline (TBR ≥1.6) showed mild but significant FDG reduction in the once and twice daily losmapimod groups compared to placebo (both ΔTBR −0.10, $p<0.02$). In support, losmapimod reduced serum inflammatory biomarkers (hsCRP, IL-8, MMP-9, MCP-1) and visceral fat FDG uptake, indicating a systemic anti-inflammatory effect. We eagerly await outcome trials to understand whether these FDG PET imaging findings will have predicted the success of losmapimod on clinical endpoints.

Limitations of FDG PET imaging of inflammation—Although linked to inflammation, the precise mechanisms underlying FDG uptake in atheroma are incompletely defined. In an elegant set of experiments, Folco et al. demonstrated that hypoxia mediates cellular FDG uptake *in vitro* (13). Cultured human cells in conditions similar to those experienced in atheroma demonstrated that hypoxia, but not pro-inflammatory cytokines, augmented macrophage glucose uptake. Furthermore, statins attenuated the hypoxia-induced macrophage glucose metabolism, while inflammatory cytokines upregulated glucose utilization in other cells, such as smooth muscle cells and endothelial cells. Therefore, mechanisms governing FDG uptake *in vivo* may be more complex than previously realized – including inflammatory cells, other metabolically active cells, and hypoxia.

Sodium ^{18}F-fluoride PET imaging of active plaque calcification

Calcification is a cardinal process in atherosclerosis and bulk calcification is associated with increased clinical risk when detected by CT or x-ray. A promising plaque calcification-targeted PET imaging agent is sodium ^{18}F-fluoride (NaF), a marker of active mineralization that has favorable pharmacokinetics and minimal non-specific soft tissue uptake, and has been clinically used to detect bone metastases. Derlin et al. examined NaF PET uptake in the common carotid arteries of 269 asymptomatic cancer patients undergoing PET-CT (14). Approximately 35% of patients demonstrated uptake of NaF in the carotid artery. NaF significantly correlated with the degree of atherosclerotic calcification on CT imaging ($r=0.85$, $p<0.0001$), although conversely not all CT-identified calcifications demonstrated NaF PET signal. NaF activity also associated with traditional cardiovascular risk factors such as hypertension, hyperlipidemia, age, and male sex. NaF is therefore a new player in atherosclerosis PET imaging, and offers new insights into atheroma progression complementary to FDG PET, as discussed next.

Comparison of FDG and NaF signals in carotid plaques—To further assess the differential topography of plaque metabolism and mineralization in atherosclerosis, Derlin et al. retrospectively reviewed 45 PET/CT studies in oncology patients who underwent both FDG and NaF PET scans within a six-month period (16). Most subjects demonstrated focal carotid and aortic vascular FDG uptake. However, calcified lesions associated preferentially with NaF rather than FDG (77% vs. 15%, respectively). Notably, the overlap between NaF and FDG signals were minimal, occurring in only 6.5% of patients, again highlighting the spatial uniqueness of inflammation and mineralization in atherosclerosis. This finding further supports that bulk calcification may represent a "burnt out" end stage of atherosclerosis.

Coronary imaging—In a remarkable advance, NaF PET also enabled the noninvasive detection of plaque mineralization in human coronary arteries (15). In a study of 119 subjects with or without calcific aortic stenosis, NaF uptake significantly associated with patients with angina, prior cardiovascular events, and traditional risk factors. NaF PET was found to correlate with the CT coronary artery calcium (CAC) score ($r=0.652$, $p<0.001$). Interestingly, a subset of patients with high CAC scores >1000 had *no* detectable NaF activity, potentially indicating more stable, end-stage calcified plaques (Figure 3). Yet this is potentially a challenge to understand NaF's role in risk prediction – as clinical CAC scores of >1000 are associated with a markedly elevated CV risk. Likely NaF is detecting earlier stage calcified lesions with ongoing mineralization.

In an NaF vs. FDG comparison study in the same patients, FDG did not associate with coronary atherosclerosis, likely due to strong background myocardial FDG uptake. Overall, NaF may allow identification of plaque calcium deposition in remodeling atheromas – potentially in the coronary bed, a major advance for noninvasive molecular imaging. The key question is whether NaF uptake will predict cardiovascular events independently beyond risk factors and the CAC – a question that is critical for every coronary atherosclerosis molecular imaging approach.

Carotid plaque inflammation imaging via new macrophage-targeted agents—A relatively new PET agent ^{11}C-PK11195 targets activated macrophages by selectively interacting with the macrophage translocator protein (TSPO, formerly known as the peripheral benzodiazepine receptor). ^{11}C-PK11195 PET/CT was performed in 32 patients with >50% carotid stenosis (17). In the 9 symptomatic patients with recent ipsilateral stroke or TIA, the ^{11}C-PK11195 plaque signal was greater compared to subjects with asymptomatic stenosis (TBR 1.06±0.20 vs. 0.86±0.11, $p=0.001$). ^{11}C-PK11195 signals corresponded well with immunostained macrophages. Additionally, the plaques of symptomatic patients exhibited relatively lower CT Hounsfield units, a feature associated with lipid-laden and high-risk lesions. CT plaque attenuation however did not correlate with ^{11}C-PK11195 activity, suggesting that structural CT and molecular PET information may be complementary approaches for plaque assessment. In combination, high ^{11}C-PK11195 signal with low CT plaque attenuation achieved a high predictive value >90% for identifying symptomatic carotid plaques in this pilot study. An important next step is to determine whether elevated ^{11}C-PK11195 signals will predict carotid plaque progression and events in asymptomatic patients. More importantly – the superiority of this agent compared to FDG will need to be demonstrated, as FDG is widely available and enjoys significant lead time in clinical applications.

Preclinical advances

Intravascular NIRF imaging: standalone NIRF and integrated OFDINIRF—Noninvasive carotid plaque molecular imaging is now established, but molecular imaging of the coronary arteries, the primary source of acute MI, is in its infancy. New approaches, particularly high-resolution intravascular approaches, are actively under development. Recent demonstrates that intravascular near-infrared fluorescence (NIRF) imaging is attractive for coronary artery molecular imaging. NIRF imaging offers high-resolution, good sensitivity, multiple imaging agent reporters, and operationally utilizes flexible optical fibers, and importantly, can enable signal detection through blood. Using a specially-designed rotational imaging fiber housed in a conventional IVUS-style catheter, Jaffer et al. demonstrated the ability to capture 2D NIRF signals through flowing blood, without flushing or vessel occlusion, in the aorta of atherosclerotic rabbits, which have a similar size as human coronary arteries (18). Rabbits injected 24 hours prior to intravascular imaging with Prosense VM110, a NIRF molecular imaging agent that detects activated proteases

(cathepsins) resident within the arterial wall, showed high NIRF inflammatory signals that colocalized with IVUS-verified plaques (Figure 4). The authors also used the 2-dimensional NIRF system to image coronary stent-induced inflammation, revealing an edge-based inflammatory pattern in bare-metal stents 7 days after implantation. Limitations of that system included the lack of co-registered anatomical information and semi-quantitative readouts – limitations addressed next.

NIRF-OFDI—Standalone NIRF is semi-quantitative due to lack of precisely co-registered positional information. Therefore, a new dual-modality NIRF-OFDI molecular-structural imaging catheter was recently developed for simultaneous and quantitative NIRF molecular imaging and anatomical OFDI, the high-speed 2nd generation optical coherence tomography (OCT) technology (19). This clinical-type catheter system enabled nanomolar NIRF detection with high-resolution OFDI microstructural data (~7μm axial spatial resolution). Moreover, the availability of positional information allowed distance correction of the NIRF signal allowing quantification of the NIRF signal to luminal boundary. Intravascular experiments in rabbits demonstrated the capability to detect fibrin deposition on stent struts and atherosclerotic plaque protease inflammatory activity. Clinical translation of NIRF catheters is planned within the next 1-2 years. This combined system is positioned to provide the first high-resolution maps of coronary inflammation, especially as NIRF molecular imaging agents are increasingly clinically available (see next section).

Indocyanine green NIRF imaging of lipid-rich, inflamed plaques—In addition to intravascular NIRF catheters, clinically targeted NIRF molecular imaging agents are needed to enable coronary NIRF molecular imaging. Vinegoni et al. evaluated using the FDA-approved agent indocyanine green (ICG) for NIRF plaque imaging in atherosclerotic rabbits (20). ICG is a long-established vascular NIRF imaging agent used for ophthalmologic, cardiac and hepatic blood flow studies, and fluoresces in the NIR. Twenty minutes after intravenous ICG injection in rabbits, ICG localized to lipid-laden, inflamed aortic plaques detected by *in vivo* intravascular NIRF sensing. *In vitro* experiments demonstrated ICG uptake was enhanced by both lipid (acetylated LDL) and macrophages. This observation was clinically supported by ICG accumulation in macrophage- and lipid-rich zones in freshly resected human CEA specimens incubated with ICG. ICG combined with intravascular NIRF catheter technology thus shows promise for future human studies of high-risk coronary arterial plaques. Challenges for NIRF imaging include the lack of specific clinical tracers for atherosclerosis, but recent developments in fluorescence molecular imaging of clinical cancer patients (e.g *Nature Medicine* 2011;17:1315-19) are expected to produce a number of clinical NIRF agents in the next 3 years.

Molecular MRI of elastin and plaque remodeling—The extracellular matrix protein elastin is an abundant component of evolving atheroma related to underlying plaque burden. With the introduction of a new low-molecular weight gadolinium-labeled elastin-specific magnetic resonance contrast agent (^{158}Gd-ESMA), elastin-rich vascular regions can now be detected noninvasively at high resolution and high SNR >10 (Figure 5) (21). In apolipoprotein-E deficient (ApoE$^{-/-}$) atherosclerotic mice, quantitative elastin vessel wall content assessed by ^{158}Gd-ESMA correlated with the time on high-cholesterol diet, and was diminished by 12 weeks of pravastatin treatment. Furthermore, plaque cross-sectional area and elastin content measured by histology and immunoblotting exhibited a strong positive relationship with ^{158}Gd-ESMA MRI contrast-enhancement (r^2>0.7 for all comparators). Another elastin-targeted MRI contrast agent being pursued to non-invasively detect atherosclerotic plaque development and remodeling, BMS-753951, also demonstrated promise to identify in-stent restenosis in injured pig coronary arteries 4 weeks after stent placement, with an excellent histology correlation with plaque volume (r^2=0.86) (22). It

remains to be determined whether elastin molecular MRI of plaque volume will provide a significant advance over coronary plaque volume imaging by the latest generation of cardiac CT scanners.

Myocardial Infarction and Thrombosis

Inflammation imaging in acute myocardial infarction

Inflammation is critical in healing an acute infarction by producing a compact scar. However, excessive inflammation may induce adverse myocardial remodeling (LV dilatation). The ability to map inflammation in human infarction could provide new insights into the time course and topography of MI-induced inflammation, and its attendant consequences. In a proof-of-principle clinical study, Alam et al. imaged myocardial inflammation via serial MRI of infarct macrophages, enabled by pre-injection of ferumoxytol, an ultrasmall superparamagnetic iron oxide (USPIO) nanoparticle. Ferumoxytol is FDA-approved for iron-deficiency anemia in patients with chronic kidney disease, but as a USPIO preparation, induces T2>T1 relaxation effects on MRI. A total of 16 patients underwent USPIO-enhanced MRI within 5 days after acute ST-elevation MI (23). T2-weighted MRI was performed at baseline without agent, and then 24 and 48 hrs following intravenous administration of 4mg/kg ferumoxytol. USPIOs induced T2-weighted signal loss in the infarcted region, and to a lesser extent in the non-infarcted remote myocardium. The overall approach offers a new method to assess the inflammatory response and LV remodeling in human subjects, and could also be useful in the study of myocarditis and cardiac transplant rejection. Future efforts will likely focus on understanding post-MI myocardial inflammatory levels and outcome (too low → LV rupture, too high → LV dilatation and CHF). Molecular imaging should help determine whether there is a sweet spot for inflammation for optimal LV remodeling, and whether post-MI therapies can be guided based on imaging.

Angiotensin receptor hybrid PET/CT imaging after myocardial infarction

Activation of the renin-angiotensin-aldosterone system (RAAS) is an important contributor to left ventricular remodeling after MI. The novel angiotensin II type 1 receptor (AT1R) PET ligand ^{11}C-KR31173 was investigated in swine MI and then in a first-in-human evaluation in 4 healthy volunteers (24). ^{11}C-KR31173 was up-regulated 1 hour after injection in the myocardium of infarcted pigs compared to healthy controls, with greatest activity in the infarct zone (myocardial retention index 8.7%/min vs. 5.8%/min, $p<0.01$). In humans,^{11}C-KR31173 also specifically localized to the normal myocardium, but at lower levels than in the infarcted and normal pig myocardium. Remarkably, human subjects re-administered ^{11}C-KR31173 the following day 3 hours after a single dose of an ARB (40 mg olmesartan) demonstrated decreased ^{11}C-KR31173 PET activity (Figure 6), although only 54% of receptors were blocked, suggesting limited specificity of this agent. Imaging of myocardial AT1R could have important clinical implications, such as optimizing the dose of angiotensin receptor blockers (ARBs) or motivating additional therapies to suppress the RAAS axis. If the current agent ^{11}C-KR31173 also demonstrates utility for CHF patients (as opposed to just normal volunteers), future studies could investigate whether upregulated AT1R expression refines prognosis beyond ejection fraction, heart failure class, B-natriuretic peptide levels, and other blood biomarkers. Comparative studies are also required to determine whether AT1R imaging offers advantages beyond molecular imaging of angiotensin converting enzyme (ACE), a critical element of the RAAS system that is upstream of AT1R and therefore may offer more sensitivity in reporting on RAAS activation.

MI preclinical advances—After acute MI, why is the risk of a recurrent event elevated in nonculprit arteries? Patients that experience acute MI are at elevated risk for future events, as high as 50% during year 1 in some studies, but the mechanisms underlying this phenomenon have not been established. Dutta et al. demonstrated that hypercholesterolemic mice subjected to MI or stroke developed larger atherosclerotic lesions with more high-risk features including macrophage infiltration and inflammatory protease activity (25). *In vivo* assessments were obtained using fluorescence molecular tomography with NIRF-targeted probes. Recruited macrophages originated from migratory progenitor cells traveling from the bone marrow to the spleen. In the splenic tissue, progenitor cells upregulated monocyte/macrophage production via extramedullary hematopoeisis. These macrophages then exited the spleen, circulated, and honed to atherosclerotic plaques, accelerating atherosclerosis. Enhanced bone marrow sympathetic nerve stimulation was the driving force behind this process. Progenitor cell release was reduced by β-blocker therapy. This important observation that MI itself accelerates plaque growth and increases plaque inflammation sheds light on why extended dual antiplatelet therapy confers a benefit on nonculprit arteries post MI.

Thrombosis preclinical imaging advances

New fibrin-targeted NIRF molecular imaging agent: Approaches that detect specific thrombus-associated molecules could more precisely define thrombosis syndromes. Hara et al. recently developed a new NIRF agent targeted to fibrin, termed FTP11-Cy7 (26). In murine deep vein thrombosis (DVT), FTP11-Cy7 rapidly accumulated in thrombi detected by intravital confocal fluorescence microscopy and noninvasive fluorescence molecular tomography, and was blocked by competitive inhibition of unlabeled probe. FTP11-Cy7 is likely translatable for use in patients, as the peptide backbone of this agent has been successfully tested in phase II clinical MRI trials. In concert with intravascular NIRF imaging (18,19), NIRF fibrin imaging is well positioned to investigate subclinical plaque rupture and mechanisms of stent thrombosis at very high resolution.

Relationship between venous thrombus inflammation and resolution in DVT: Similar to MI, inflammation stabilizes acutely formed DVT, but excessive inflammation may cause bystander vein wall injury and increase the risk of the post-thrombotic syndrome (PTS). Methods to image inflammation in DVT could shed important light on these outcomes. Using intravital confocal fluorescence microscopy, Ripplinger and Kessinger et al. serially assessed thrombus inflammation with fluorescent macrophage and MMP activity agents in chemical DVT (27). The degree of macrophage and MMP inflammation at day 4 predicted the amount of thrombus reduction (area) at day 6 ($p<0.05$). Thus it is plausible that methods that quantify DVT inflammation could provide prognostic information into the risk of PTS, a common and morbid syndrome following DVT.

Stem cell therapies

Evolution of two delivery methods in patients: Stem cell technologies offer great potential for therapeutic myocardial repair following acute MI, but *in vivo* mechanisms governing stem cell targeting, retention, and therapeutic effects remain unknown. To provide new insights into the comparative retention of two myocardial stem cell delivery strategies, Musialek et al. employed molecular imaging in acute MI patients receiving autologous hematopoietic stem cells shortly after MI (28). The authors compared intracoronary distal stop-flow injection through an inflated over-the-wire (OTW) coronary angioplasty balloon to a novel, non-occlusive geometrically optimized side-hole cell delivery perfusion catheter (PC). 34 subjects were randomized in a 2:1 fashion to PC or OTW stem cell delivery within 14 days of acute anterior MI treated with percutaneous coronary intervention (LVEF 22-44%). With the catheter tip positioned in the recently placed LAD stent, ~4×10^6 $CD34^+$

stem cells labeled exogenously with ^{99m}Tc-exametazime were administered selectively to the injured coronary vascular bed. At 1 hour, SPECT identified only 4.9% (OTW) and 5.1% (PC) of the initial ^{99m}Tc extametazime cell population, with cells limited almost exclusively to the (viable) peri-infarct zone as determined by myocardial perfusion imaging. Despite a non-significant difference in stem cell targeting between the two techniques, the non-occlusive PC group experienced no injection intolerance or ventricular arrhythmias, as opposed to the occlusive OTW delivery approach that required minutes of coronary flow arrest. Compared to longer-term gene reporter cell tracking strategies, exogenous labels are most useful to assess the early success of stem cell delivery since they may degrade or transfer out of the cell over time.

Vasculitis, Dissection, and Aneurysm

Large vessel vasculitis

Inflammatory vasculitidies such as Takayasu's Arteritis and Giant Cell Arteritis are important causes of organ ischemia and infarction. Mechanisms to understand the pathogenesis of these diseases in patients are needed. Vascular inflammation was evaluated in 78 consecutive patients with suspected large-vessel vasculitis using FDG PET/CT (29). After stratification by clinical diagnosis, 16 patients with steroid-naïve vasculitis exhibited greater FDG uptake in the thoracic aorta, subclavian and carotid arteries than in 18 vasculitis patients on steroid treatment. Linear regression analysis revealed a positive correlation between serum inflammatory biomarkers (CRP, ESR) and thoracic aorta FDG activity (β 0.018-0.02, $p<0.05$). In 27 Takayasu arteritis subjects with active disease, FDG activity was similarly greater than patients with inactive disease or control patients (max SUV 2.7 vs. 1.9 vs. 1.8, $p<0.001$) (30). Furthermore, those patients with relapsing disease on immunosuppressive treatment had higher FDG activity compared to those with treated stable disease (max SUV 2.6 vs. 1.9, $p<0.001$). Therefore, FDG inflammatory activity detects large vessel vasculitis activity, correlates with treatment response, and may also facilitate earlier detection of disease and monitoring of the response to therapy.

Dissection

In a consecutive series of 37 patients with spontaneous cervical artery dissection, FDG PET demonstrated local inflammation at the dissection site in >80% of patients (31). Interestingly about 20% of patients showed more extensive generalized vessel wall FDG uptake away from the local dissection site, suggesting that an inflammatory arteriopathy may have been present *before* the dissection occurred. FDG PET/CT documented diffuse inflammatory changes in more patients than 3T contrast-enhanced MRI (24% vs. 14%). All MRI-positive sites were also positive on FDG PET (3 out of 3), but not vice versa (only 4 out of 7), suggesting that FDG may be more sensitive the CE-MRI. Whether the degree of inflammation predicts arterial remodeling and aneurysm formation, or atheroma formation, remains to be determined.

Aneurysm

Can we better identify aneurysms that might rapidly progress, dissect, or rupture?

Abdominal aortic aneurysm (AAA)—Using USPIO-enhanced molecular 3T MRI, Richards et al. investigated relationships between AAA inflammation and subsequent aneurysm growth. 29 asymptomatic patients with AAA (range 4.0 to 6.6 cm diameter) underwent intravenous administration of the USPIO Sinerem (ferumoxtran, not yet FDA- or EMA-approved), followed by T2-weighted imaging of AAA macrophages (32). While all subjects demonstrated periluminal USPIO accumulation in a similar distribution to gadolinium enhancement, possibly due to layering thrombus, some patients exhibited more

deeply located mural signal (Figure 7). Despite similar aneurysm sizes, patients with USPIO deposition in the wall away from the periluminal thrombus zones had a 3-fold higher aneurysm growth rate (0.66 cm/year) compared to other patients (p=0.02). If validated in larger and multicenter studies, USPIO MRI could better identify patients suitable for conservative therapy, or for early surgical therapy, or for targeted enrollment in anti-inflammatory clinical trials.

Cerebral aneurysms—11 patients with cerebral aneurysms were also imaged with USPIO to determine the feasibility of intracranial aneurysm inflammation detection in humans (33). 72 hours after ferumoxytol 5mg/kg i.v., 78% of the aneurysms demonstrated USPIO signal loss by MRI, and post-operative analysis revealed macrophage and iron staining in the resected aneurysm tissue. Both USPIO MRI and FDG PET now provide opportunities to track inflammation in aneurysms, and outcome and comparison studies are anticipated in the next several years.

Valvular Disease

Aortic stenosis

To address the relationship between aortic valve inflammation and stenosis, FDG PET/CT studies were retrospectively reviewed in 42 oncology patients with echocardiography-defined mild, moderate, or severe degenerative AS, and in an equal number of age-matched controls (34). To minimize the bleed-through of FDG signal from the adjacent myocardium and aortic wall, signal analyses were performed with a 5 mm^3 voxel centered over the leaflet coaptation point. Both mild and moderate AS patients had significantly elevated aortic valve FDG signal compared to controls (TBR 1.50 and 1.67, respectively; TBR 1.35 in controls; $p \leq 0.01$). Similar findings were present when aortic valves were stratified by mild or moderate CT calcification (Figure 8). However, in patients with severe calcification or severe AS, FDG activity was similar to controls, suggesting these conditions are at the end stage of the inflammatory process. Furthermore, in a subgroup of 19 patients with serial echocardiographic studies over 1-2 years, subjects with a high baseline FDG signal showed AS progression in 82% of the group, whereas subjects with lower FDG baseline signal showed progression in only 22% of the group (p=0.04). FDG PET may therefore be able to discriminate patients at risk of more rapid progression of AS; and excitingly, suggests the potential for early anti-inflammatory therapies to slow the progression of AS. Prospective studies are indicated.

A second study also demonstrated greater FDG activity in the aortic valves of 121 patients with increasing severity stenosis (35). NaF activity was simultaneously assessed, with 91% of patients with AS demonstrating NaF signal uptake. Intriguingly, NaF correlated with the degree of AS more strongly than FDG (r^2=0.54 vs. 0.218, both $p<0.001$). Correlation between FDG and NaF furthermore was weak (r^2=0.174, $p<0.001$), suggesting different biological processes may be operative during valvular stenosis. While the SEAS trial of statin plus ezetimibe therapy to prevent AS progression was negative, selection of patients with active remodeling (via FDG and/or NaF) might identify a population that could derive benefit from such a therapy, or potentially other anti-inflammatory or anti-mineralization therapies.

Device Complications and Infections

FDG PET identification of device infections

Implantable cardiovascular device (ICD) infections are insidious complications that can be difficult to definitively diagnose, and lead to considerable uncertainly regarding whether explantation of the ICD is required. To establish patterns of inflammation associated with

device infections, FDG PET imaging was utilized in the following patients: (1) N=42 with suspected device infection, (2) N=12 with recent device implantation but no evidence of infection, and (3) N=12 with uncomplicated device implantation >6 months early (36). Nearly 75% of those patients with suspected device infection had positive FDG uptake, primarily at the device periphery, and 24 patients had their devices explanted with *ex vivo* documentation of device infection. 6 patients were treated for a superficial infection that resolved without device removal, and 10 patients with no FDG uptake were given antibiotic therapy without relapse at >1 year. Subjects with recent device placement without known infection had mild uptake on FDG PET/CT scans at the connector, but devices implanted >6 months prior exhibited no observed FDG signal. Thus, FDG can discriminate post-implantation device inflammation from true infection. If validated in larger studies, FDG PET could vitally guide decisions between conservative antibiotic therapy and device explanation.

Preclinical advances

Molecular imaging of bacterial endocarditis—Early detection of infective endocarditis (IE) to guide appropriate targeted antibiotic and surgical intervention is often a significant challenge, but remains key to minimizing subsequent complications such as paravalvular abscess, septic emboli, and valve dehiscence. Panizzi et al. formulated ^{64}Cu-DTPAProT, a novel prothrombin analog for PET imaging that exploits the natural bacterial host-defense mechanism of coagulase-positive *Staphlococcus aureus*, a highly destructive endovascular pathogen, by binding to the staphlocoagulase enzyme (37). Coagulase-positive *Staphlococcus aureus* aortic valve vegetations in mice were highly detectable by ^{64}Cu-DTPA ProT PET/CT imaging, but not coagulase-negative strains. Importantly for potential future clinical translation, there was no evidence of animal toxicity or clotting disorders observed from the agent. Given the clinical need for better diagnostic tools, targeted bacterial agents such as ^{64}Cu-DTPA-ProT are likely to be highly translatable for diagnostic, and possibly even theranostic (diagnostic+therapeutic) infective endocarditis management. Another potential exciting scenario is in the detection of culture-negative IE, a vexing clinical problem. Ideally, given that a number of organisms can cause IE, imaging agents that offer multiplexed detection are likely to be more useful for clinical diagnostics.

Supplement

Please see supplement for additional advances in the areas of atherosclerosis, cardiomyopathy, thrombosis, allograft rejection, vascular injury, and endocarditis.

Outlook

The rapid growth of cardiovascular molecular imaging has expanded our ability to understand disease biology *in vivo*. While FDG PET atherosclerosis imaging remains at the forefront of this field, new clinical imaging approaches are expanding in this area as well as in cardiomyopathy, vasculitis, valvular disease, aortic aneurysm and dissection, and myocardial infarction. Continued progress in human clinical cardiovascular molecular imaging studies is anticipated, as recently witnessed over the period of this review series. In particular, clinical molecular imaging trials are now focusing on how molecular information can improve risk stratification beyond traditional structural imaging and routine clinical biomarkers – a key aspect that will define the long-term utility of cardiovascular molecular imaging.

Supplementary Material

Refer to Web version on PubMed Central for supplementary material.

Acknowledgments

Funding Sources: NIH R01 HL108229, American Heart Association Scientist Development Grant #0830352N and Grant-in-Aid #13GRNT1760040, and Howard Hughes Medical Institute Career Development Award.

References

1. Buxton DB, Antman M, Danthi N, et al. Report of the National Heart, Lung, and Blood Institute working group on the translation of cardiovascular molecular imaging. Circulation. 2011; 123:2157–63. [PubMed: 21576680]
2. Bucerius J, Duivenvoorden R, Mani V, et al. Prevalence and risk factors of carotid vessel wall inflammation in coronary artery disease patients: FDG-PET and CT imaging study. JACC Cardiovasc Imaging. 2011; 4:1195–205. [PubMed: 22093271]
3. Bucerius J, Mani V, Moncrieff C, et al. Impact of noninsulin-dependent type 2 diabetes on carotid wall 18F-fluorodeoxyglucose positron emission tomography uptake. J Am Coll Cardiol. 2012; 59:2080–8. [PubMed: 22651864]
4. Myers KS, Rudd JH, Hailman EP, et al. Correlation between arterial FDG uptake and biomarkers in peripheral artery disease. JACC Cardiovasc Imaging. 2012; 5:38–45. [PubMed: 22239891]
5. Figueroa AL, Subramanian SS, Cury RC, et al. Distribution of inflammation within carotid atherosclerotic plaques with high-risk morphological features: a comparison between positron emission tomography activity, plaque morphology, and histopathology. Circ Cardiovasc Imaging. 2012; 5:69–77. [PubMed: 22038986]
6. Fifer KM, Qadir S, Subramanian S, et al. Positron emission tomography measurement of periodontal (18)f-fluorodeoxyglucose uptake is associated with histologically determined carotid plaque inflammation. J Am Coll Cardiol. 2011; 57:971–6. [PubMed: 21329844]
7. Yoo HJ, Kim S, Park MS, et al. Vascular inflammation stratified by C-reactive protein and low-density lipoprotein cholesterol levels: analysis with 18F-FDG PET. J Nucl Med. 2011; 52:10–7. [PubMed: 21149476]
8. Mizoguchi M, Tahara N, Tahara A, et al. Pioglitazone attenuates atherosclerotic plaque inflammation in patients with impaired glucose tolerance or diabetes a prospective, randomized, comparator-controlled study using serial FDG PET/CT imaging study of carotid artery and ascending aorta. JACC Cardiovasc Imaging. 2011; 4:1110–8. [PubMed: 21999871]
9. Chang K, Francis SA, Aikawa E, et al. Pioglitazone suppresses inflammation in vivo in murine carotid atherosclerosis: novel detection by dual-target fluorescence molecular imaging. Arterioscler Thromb Vasc Biol. 2010; 30:1933–9. [PubMed: 20689078]
10. Vucic E, Dickson SD, Calcagno C, et al. Pioglitazone modulates vascular inflammation in atherosclerotic rabbits noninvasive assessment with FDG-PET-CT and dynamic contrast-enhanced MR imaging. JACC Cardiovasc Imaging. 2011; 4:1100–9. [PubMed: 21999870]
11. Fayad ZA, Mani V, Woodward M, et al. Safety and efficacy of dalcetrapib on atherosclerotic disease using novel non-invasive multimodality imaging (dal-PLAQUE): a randomised clinical trial. Lancet. 2011; 378:1547–59. [PubMed: 21908036]
12. Elkhawad M, Rudd JH, Sarov-Blat L, et al. Effects of p38 mitogen-activated protein kinase inhibition on vascular and systemic inflammation in patients with atherosclerosis. JACC Cardiovasc Imaging. 2012; 5:911–22. [PubMed: 22974804]
13. Folco EJ, Sheikine Y, Rocha VZ, et al. Hypoxia but not inflammation augments glucose uptake in human macrophages: Implications for imaging atherosclerosis with 18fluorine-labeled 2-deoxy-D-glucose positron emission tomography. J Am Coll Cardiol. 2011; 58:603–14. [PubMed: 21798423]
14. Derlin T, Wisotzki C, Richter U, et al. In vivo imaging of mineral deposition in carotid plaque using 18F-sodium fluoride PET/CT: correlation with atherogenic risk factors. J Nucl Med. 2011; 52:362–8. [PubMed: 21321276]
15. Dweck MR, Chow MW, Joshi NV, et al. Coronary arterial 18F-sodium fluoride uptake: a novel marker of plaque biology. J Am Coll Cardiol. 2012; 59:1539–48. [PubMed: 22516444]

16. Derlin T, Toth Z, Papp L, et al. Correlation of inflammation assessed by 18F-FDG PET, active mineral deposition assessed by 18F-fluoride PET, and vascular calcification in atherosclerotic plaque: a dual-tracer PET/CT study. J Nucl Med. 2011; 52:1020–7. [PubMed: 21680686]
17. Gaemperli O, Shalhoub J, Owen DR, et al. Imaging intraplaque inflammation in carotid atherosclerosis with 11C-PK11195 positron emission tomography/computed tomography. Eur Heart J. 2012; 33:1902–10. [PubMed: 21933781]
18. Jaffer FA, Calfon MA, Rosenthal A, et al. Two-dimensional intravascular near-infrared fluorescence molecular imaging of inflammation in atherosclerosis and stent-induced vascular injury. J Am Coll Cardiol. 2011; 57:2516–26. [PubMed: 21679853]
19. Yoo H, Kim JW, Shishkov M, et al. Intra-arterial catheter for simultaneous microstructural and molecular imaging in vivo. Nat Med. 2011; 17:1680–4. [PubMed: 22057345]
20. Vinegoni C, Botnaru I, Aikawa E, et al. Indocyanine green enables near-infrared fluorescence imaging of lipid-rich, inflamed atherosclerotic plaques. Sci Transl Med. 2011; 3:84ra45.
21. Makowski MR, Wiethoff AJ, Blume U, et al. Assessment of atherosclerotic plaque burden with an elastin-specific magnetic resonance contrast agent. Nat Med. 2011; 17:383–8. [PubMed: 21336283]
22. von Bary C, Makowski M, Preissel A, et al. MRI of coronary wall remodeling in a swine model of coronary injury using an elastin-binding contrast agent. Circ Cardiovasc Imaging. 2011; 4:147–55. [PubMed: 21378029]
23. Alam SR, Shah AS, Richards J, et al. Ultrasmall superparamagnetic particles of iron oxide in patients with acute myocardial infarction: early clinical experience. Circ Cardiovasc Imaging. 2012; 5:559–65. [PubMed: 22875883]
24. Fukushima K, Bravo PE, Higuchi T, et al. Molecular hybrid positron emission tomography/computed tomography imaging of cardiac angiotensin II type 1 receptors. J Am Coll Cardiol. 2012; 60:2527–34. [PubMed: 23158533]
25. Dutta P, Courties G, Wei Y, et al. Myocardial infarction accelerates atherosclerosis. Nature. 2012; 487:325–9. [PubMed: 22763456]
26. Hara T, Bhayana B, Thompson B, et al. Molecular imaging of fibrin deposition in deep vein thrombosis using fibrin-targeted near-infrared fluorescence. JACC Cardiovasc Imaging. 2012; 5:607–15. [PubMed: 22698530]
27. Ripplinger CM, Kessinger CW, Li C, et al. Inflammation modulates murine venous thrombosis resolution in vivo: assessment by multimodal fluorescence molecular imaging. Arterioscler Thromb Vasc Biol. 2012; 32:2616–24. [PubMed: 22995524]
28. Musialek P, Tekieli L, Kostkiewicz M, et al. Randomized transcoronary delivery of CD34(+) cells with perfusion versus stop-flow method in patients with recent myocardial infarction: Early cardiac retention of (9)(9)(m)Tc-labeled cells activity. J Nucl Cardiol. 2011; 18:104–16. [PubMed: 21161463]
29. Papathanasiou ND, Du Y, Menezes LJ, et al. 18F-Fludeoxyglucose PET/CT in the evaluation of large-vessel vasculitis: diagnostic performance and correlation with clinical and laboratory parameters. Br J Radiol. 2012; 85:e188–94. [PubMed: 21385914]
30. Tezuka D, Haraguchi G, Ishihara T, et al. Role of FDG PET-CT in Takayasu arteritis: sensitive detection of recurrences. JACC Cardiovasc Imaging. 2012; 5:422–9. [PubMed: 22498333]
31. Pfefferkorn T, Saam T, Rominger A, et al. Vessel wall inflammation in spontaneous cervical artery dissection: a prospective, observational positron emission tomography, computed tomography, and magnetic resonance imaging study. Stroke. 2011; 42:1563–8. [PubMed: 21512185]
32. Richards JM, Semple SI, MacGillivray TJ, et al. Abdominal aortic aneurysm growth predicted by uptake of ultrasmall superparamagnetic particles of iron oxide: a pilot study. Circ Cardiovasc Imaging. 2011; 4:274–81. [PubMed: 21304070]
33. Hasan DM, Mahaney KB, Magnotta VA, et al. Macrophage imaging within human cerebral aneurysms wall using ferumoxytol-enhanced MRI: a pilot study. Arterioscler Thromb Vasc Biol. 2012; 32:1032–8. [PubMed: 22328774]
34. Marincheva-Savcheva G, Subramanian S, Qadir S, et al. Imaging of the aortic valve using fluorodeoxyglucose positron emission tomography increased valvular fluorodeoxyglucose uptake in aortic stenosis. J Am Coll Cardiol. 2011; 57:2507–15. [PubMed: 21679852]

35. Dweck MR, Jones C, Joshi NV, et al. Assessment of valvular calcification and inflammation by positron emission tomography in patients with aortic stenosis. Circulation. 2012; 125:76–86. [PubMed: 22090163]

36. Sarrazin JF, Philippon F, Tessier M, et al. Usefulness of fluorine-18 positron emission tomography/computed tomography for identification of cardiovascular implantable electronic device infections. J Am Coll Cardiol. 2012; 59:1616–25. [PubMed: 22538331]

37. Panizzi P, Nahrendorf M, Figueiredo JL, et al. In vivo detection of Staphylococcus aureus endocarditis by targeting pathogen-specific prothrombin activation. Nat Med. 2011; 17:1142–6. [PubMed: 21857652]

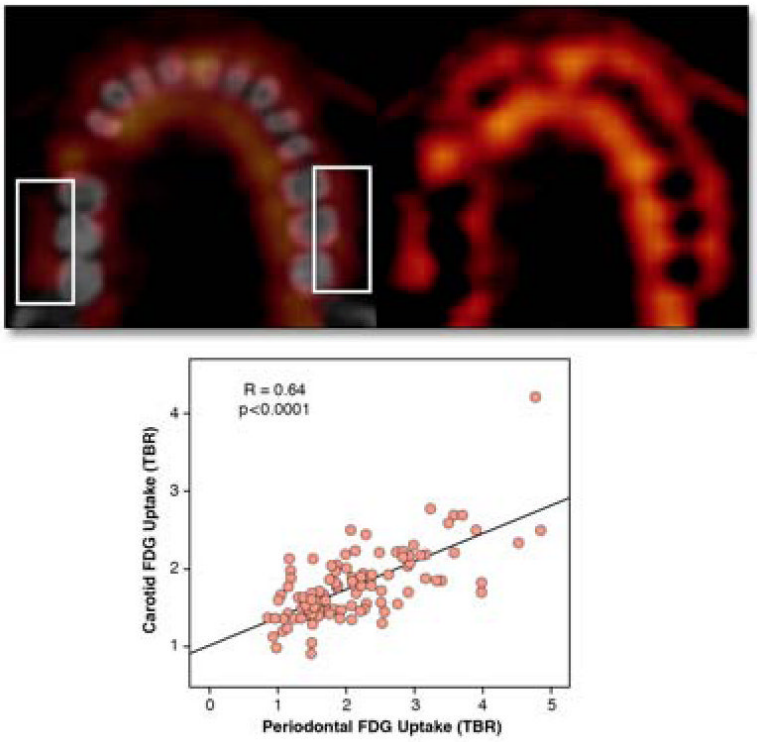

Figure 1. Periodontal FDG-PET

PET (top, right) and PET-CT fusion (top, left) images reveal high FDG uptake in periodontal tissues (boxes indicate measurement regions). Quantitative TBR of periodontal FDG activity significantly correlated with carotid FDG uptake. Reproduced with permission from (6).

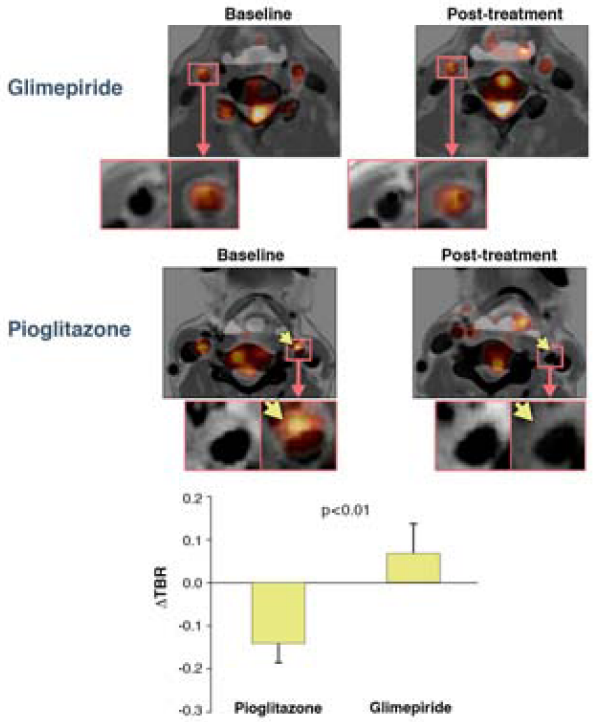

Figure 2. Effect of pioglitazone and glimepiride on atherosclerotic plaque FDG uptake

FDG PET-CT images from representative patients treated at baseline (left) or following 4 months treatment (right) with pioglitazone or glimepiride. Arrows indicate an area of reduced FDG uptake in the pioglitazone arm. Reproduced with permission from (8).

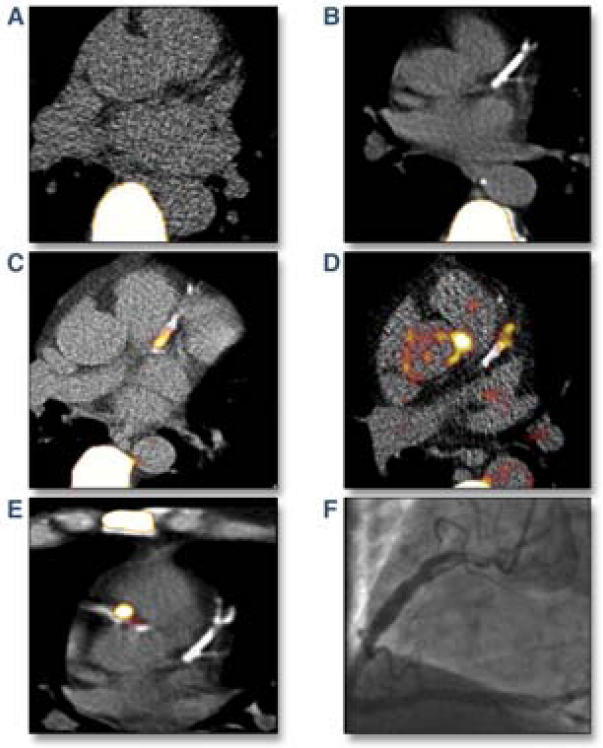

Figure 3. Coronary artery 18F-sodium fluoride (NaF) PET/CT imaging

(A) A control group patient with absent coronary artery calcium and no coronary NaF PET activity. Note the significant vertebral body NaF uptake. (B) Despite extensive left anterior descending (LAD) calcification, coronary NaF signal is not present in this subject. (C, D) Examples of patients with significant NaF PET activity and CT coronary calcification in the proximal and mid LAD. (E) Heightened NaF coronary PET uptake in the culprit proximal right coronary artery (RCA) of a patient after recent inferior non-ST elevation myocardial infarction. Note the absence of LAD NaF PET signal. (F) Coronary angiography in the patient from (E) demonstrated an ulcerated, thrombotic proximal RCA lesion. Reproduced with permission from (15).

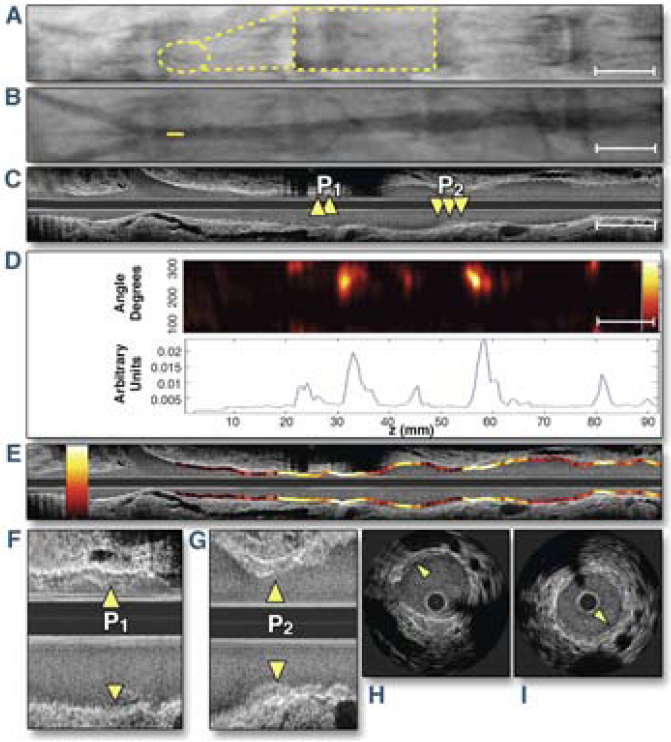

Figure 4. Intravascular NIRF imaging of protease inflammation in experimental atherosclerosis

(A, B) Fluoroscopic and angiographic images (A, yellow dotted lines: high magnification inset of the radiopaque tip of the catheter; B, solid yellow line: intravascular catheter tip position) positioned in the rabbit aorta, proximal to the iliac bifurcation. (C) Co-registered longitudinal IVUS demonstrates mild aortic plaques P1 and P2. (D) NIRF catheter pullback aligned with images A through C reveals NIRF protease activity at mild plaques (top) with 1-dimensional angle-averaged NIRF plot (bottom). (E) Superimposed longitudinal IVUS and NIRF fusion images (NIRF scale bar: yellow/white=strong, red/black=weak). (F, G) Longitudinal and (H, I) axial images of plaques P1 and P2. Reproduced with permission from (18).

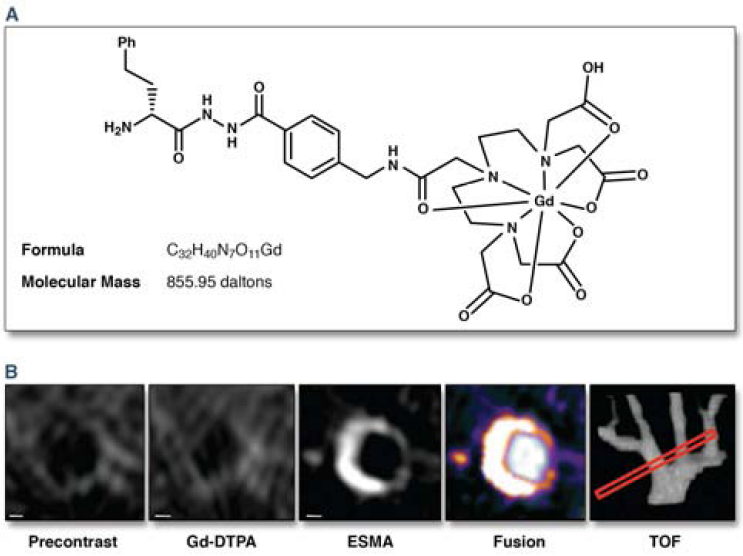

Figure 5. Elastin-targeted MRI of murine atherosclerotic plaque remodeling with ^{158}Gd-ESMA

(a) ^{158}Gd-ESMA chemical structure and formula. (b) ApoE$^{-/-}$ mouse brachiocephalic cross-sectional time-of-flight (TOF) angiography alignment (red box) comparing baseline (precontrast) with high-resolution contrast MRI (Gd-DTPA), ^{158}Gd-ESMA, and TOF/dynamic contrast (fusion) images. Scale bars, 250 m. Reproduced with permission from (21).

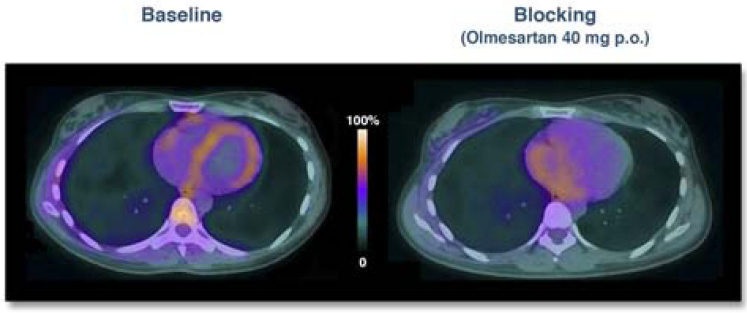

Figure 6. Human myocardial angiotensin II receptor PET/CT imaging

Mid-cardiac PET/CT fusion images in a healthy volunteer obtained 1 hour after injection with the angiogensin II type I receptor ligand ^{11}C-KR31173. (Left) At baseline, ^{11}C-KR31173 signal localizes to the ventricular myocardium. (Right) 3 hours after administration of a single 40 mg PO dose of the angiotensin receptor blocker olmesartan, myocardial ^{11}C-KR31173 PET uptake is significantly reduced. Reproduced with permission from (24).

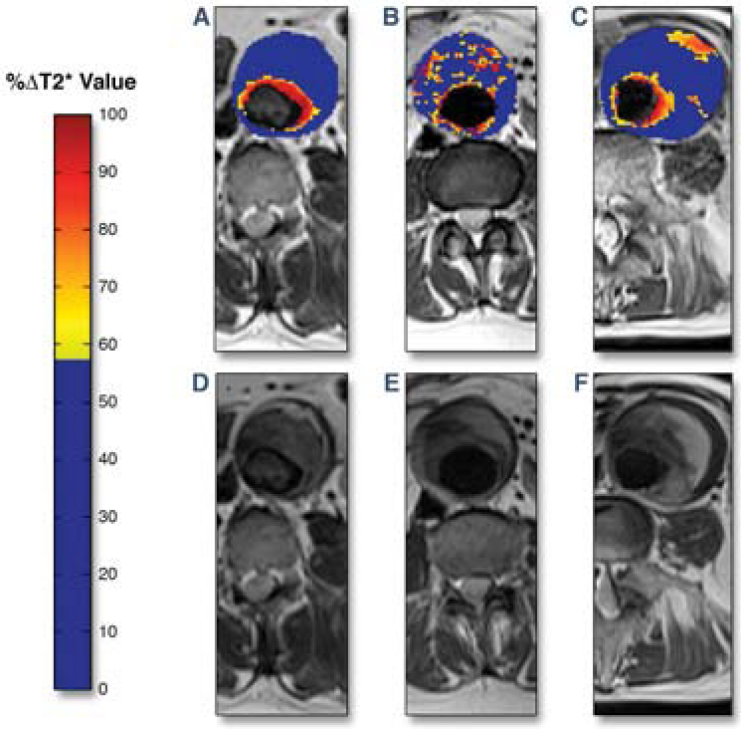

Figure 7. MRI molecular imaging of inflammation in abdominal aortic aneurysm (AAA)

Representative color maps of T2-weighted MRI signal change (blue=low, red=high) induced by local accumulation of ultrasmall superparamagnetic particles of iron oxide (USPIO) in 3 patients with AAA. (A) A patient with enhanced periluminal T2 signal. (B) More diffuse, non-contiguous T2 changes present within the intraluminal thrombus, but not involving the aortic wall. (C) Periluminal T2 signal change with focal aortic T2 enhancement revealing USPIO accumulation and inflammation within the AAA wall. (D-E) T2-weighted MRI images without the superimposed color maps for comparison demonstrating focal T2 signal loss at USPIO-rich sites. Reproduced with permission from (32).

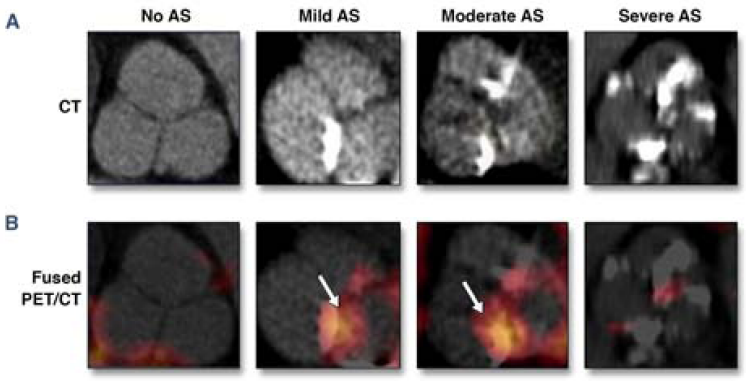

Figure 8. Clinical FDG PET imaging of inflammation in aortic stenosis

(A) CT-determined aortic valve calcification at differing AS severities. (B) Co-registered FDG PET/CT fusion demonstrates increased FDG valve uptake for mild and moderate AS (arrows), that diminishes for heavily calcified severe AS. Reproduced with permission from (34).

Table 1

Clinically targeted molecular imaging agents (partial list)

Agent	Modality	Primary Target	Application	Clinically
FDG (^{18}F-fluorodeoxyglucose)	PET	Glucose transporter-1, hexokinase	Atherosclerosis, Aneurysm, Vasculitis (Metabolism)	Yes
NaF (^{18}F-sodium fluoride)	PET	Hydroxyapatite	Atherosclerosis (Calcification)	Yes
^{11}C-acetate	PET	Fatty acid synthetase	Atherosclerosis (Fatty acids)	Yes
[^{11}C]-(R)-PK11195	PET	Benzodiazepine receptor/macrophages	Vasculitis (Inflammation)	Yes
^{11}C-KR31173	PET	Angiotensin II type I receptor	Myocardial Infarction, Cardiomyopathy (Remodeling)	Yes
^{18}F-EF5	PET	Hypoxic cells	Atherosclerosis (Inflammation)	Yes
^{64}Cu-DTPA-ProT	PET	Staphlocoagulase	Endocarditis (Vegetations)	No
^{99m}Tc-annexin V	SPECT	Annexin/macrophages	Myocardial Infarction, Cardiomyopathy (Apoptosis)	Yes
^{99m}Tc-RIP (radiolabeled RGD imaging peptide)	SPECT	$\alpha_v\beta_3$ integrins	Myocardial Infarction (Fibrosis)	Yes
^{99m}Tc-exametazime leukocytes	SPECT	White blood cells	Transplant (Inflammation)	Yes
^{111}In-RP782	SPECT	Matrix metalloproteinases	Atherosclerosis (Inflammation)	No
^{99m}Tc-RP805	SPECT	Matrix metalloproteinases	Atherosclerosis (Inflammation)	No
^{99m}Tc-fucoidin	SPECT	P-selectin	Atherosclerosis, Thrombosis, Endocarditis (Inflammation)	No
^{99m}Tc-NC100692	SPECT	$\alpha_v\beta_3$ integrins	Vascular injury (Inflammation)	No
N1177	CT	Macrophages	Atherosclerosis (Inflammation)	No
P-selectin microbubbles	Ultrasound	P-selectin	Vascular injury (Inflammation)	No
Supravist (SHU 555 C)	MRI	Macrophages	Atherosclerosis (Inflammation)	Yes
SPIO / USPIO	MRI	Macrophages	Atherosclerosis (Inflammation)	Yes
EP-2104R	MRI	Fibrin	Thrombosis (Coagulation)	Yes
P947	MRI	Matrix metalloproteinases	Atherosclerosis (Inflammation)	No
FeCo/graphite nanocrystals	MRI	Macrophages	Atherosclerosis (Inflammation)	No
^{158}Gd-ESMA	MRI	Elastin	Atherosclerosis (Plaque burden)	No

Agent	Modality	Primary Target	Application	Clinically
BMS-753951	MRI	Elastin	Atherosclerosis (Plaque burden)	No
CNA-35	MRI	Collagen	Aneurysm (Extracellular matrix)	No
Gd-TO	MRI	DNA	Myocardial Infarction (Necrosis)	No
VS-580H	MRI	Macrophages	Transplant (Inflammation)	No
SPIO-labeled EPC	MRI	Endothelial progenitor cells	Transplant (Cell tracking)	No
Human ferritin cages	MRI, NIRF	Macrophages	Atherosclerosis (Inflammation)	No
$\alpha_v\beta_3$-targeted nanoparticles	MRI, NIRF	$\alpha_v\beta_3$ integrins	Atherosclerosis (Neovessels)	No
$_{18}$F-CLIO	MRI, NIRF	Macrophages	Atherosclerosis, aneurysm (Inflammation)	No
ICG (indocyanine green)	NIRF	Lipids/macrophages	Atherosclerosis (Inflammation)	Yes
ProSense	NIRF	Cysteine proteases	Atherosclerosis (Inflammation)	No
MMPsense	NIRF	Matrix metalloproteinases	Atherosclerosis (Inflammation)	No
FTP11-Cy7	NIRF	Fibrin	Thrombosis (Coagulation)	No